Journal of ELECTRONIC MATERIALS
DOI: 10.1007/s11664-010-1256-7

Nanostructured Interfaces for Thermoelectrics

Y. GAO,[1,4] A.M. MARCONNET,[1] M.A. PANZER,[1] S. LEBLANC,[1] S. DOGBE,[2] Y. EZZAHRI,[3] A. SHAKOURI,[3] and K.E. GOODSON[1]

1.—Mechanical Engineering Department, Stanford University, Stanford, CA 94305, USA. 2.—Stanford Nanofabrication Facility, Stanford, CA 94305, USA. 3.—Baskin School of Engineering, University of California at Santa Cruz, Santa Cruz, CA 95064, USA. 4.—e-mail: yuangao@stanford.edu

Temperature drops at the interfaces between thermoelectric materials and the heat source and sink reduce the overall efficiency of thermoelectric systems. Nanostructured interfaces based on vertically aligned carbon nanotubes (CNTs) promise the combination of mechanical compliance and high thermal conductance required for thermoelectric modules, which are subjected to severe thermomechanical stresses. This work discusses the property requirements for thermoelectric interface materials, reviews relevant data available in the literature for CNT films, and characterizes the thermal properties of vertically aligned multiwalled CNTs grown on a candidate thermoelectric material. Nanosecond thermoreflectance thermometry provides thermal property data for 1.5-μm-thick CNT films on SiGe. The thermal interface resistances between the CNT film and surrounding materials are the dominant barriers to thermal transport, ranging from 1.4 m^2 K MW^{-1} to 4.3 m^2 K MW^{-1}. The volumetric heat capacity of the CNT film is estimated to be 87 kJ m^{-3} K^{-1}, which corresponds to a volumetric fill fraction of 9%. The effect of 100 thermal cycles from 30°C to 200°C is also studied. These data provide the groundwork for future studies of thermoelectric materials in contact with CNT films serving as both a thermal and electrical interface.

Key words: Thermal interface materials, thermoelectric modules, thermoreflectance thermometry, vertically aligned carbon nanotubes, silicon germanium, thermomechanical stress

Nomenclature

c_p	Heat capacity, J kg^{-1} K^{-1}
C_v	Volumetric heat capacity, J m^{-3} K^{-1}
D	Bond line thickness, μm
f_{eff}	Effective fill fraction of CNT film, %
G	Shear modulus, GPa
k	Thermal conductivity, W m^{-1} K^{-1}
L	Joint length, m
R	Thermal resistivity, m K W^{-1}
R''	Thermal resistance, m^2 K W^{-1}
ΔT	Temperature excursion, K

Greek symbols

α	Thermal expansion coefficient, 10^{-6} K^{-1}
ρ	Density of CNT, kg m^{-3}
σ	Maximum shear stress, GPa

Subscripts

1	Thermal expansion coefficient of layer 1
2	Thermal expansion coefficient of layer 2
CNT-Pt	Boundary between CNT film and Pt metal layer
CNT-Sub	Boundary between CNT film and substrate
eff	Effective
ind	Individual
tot	Total

INTRODUCTION

Efficient thermoelectric modules (TEMs) require low thermal resistances at the interfaces between the functional materials, the electrodes, and the

(Received July 21, 2009; accepted April 22, 2010)

Published online: 23 June 2010

heat exchangers. These interfaces must also accommodate the significant coefficient of thermal expansion (CTE) mismatch between these regions in the device. The repetitive temperature differences experienced by TEMs can exceed 1000 K, and the resulting thermal stress can degrade the quality of the interface and increase the interface thermal resistance over the module lifetime.[1,2]

Past work demonstrated the importance of interface resistances for thermoelectric modules as well as the need for detailed thermomechanical modeling.[3–6] Pettes et al.[7] used one-dimensional electrothermal simulations to show that, when the thermal contact conductance is decreased by a factor of 10, heat removal by a thermoelectric cooler decreases by at least 10%. LeBlanc and Gao[8] showed that thermal interface resistances reduced the attainable electrical power output of a thermoelectric generator (TEG) in a water heater by 30% to 50%. The importance of thermomechanical studies of TEMs is emphasized in several recent works. Clin et al.[9] modeled stresses in TEMs due to temperature gradients across thermoelectric pellets, anisotropic CTE of the thermoelectric material, and CTE mismatch between different materials. Hori et al.[10] demonstrated decreasing power output and eventual breakdown of TEMs due to deterioration of interfaces after thermal cycling. These effects necessitate a mechanically compliant and thermally conducting thermal interface material (TIM).

There has been extensive research on TIMs for microprocessors. The temperature fluctuations experienced by microprocessors are generally much less than those experienced by TEMs, allowing the use of thinner interface layers and relatively stiff materials such as metal alloys. Common interface materials include greases, solders, and polymer-based composites.[11] The thermoelectric community typically uses these commercially available TIMs. Recently there has been interest in nanostructured TIMs composed of carbon nanotubes (CNTs). TIMs made of both homogeneous CNT–polymer composites and vertically aligned CNT arrays may perform as an exceptional thermal interface material because they have both high thermal conductivity and mechanical compliance.[12,13] While individual nanotubes are known to have high stiffness, characterization of arrays of nanotubes has shown comparatively low axial elastic modulus due to the low packing density of the CNT array and large aspect ratio of individual tubes.[14] CNT arrays can currently be grown up to millimeters in height and over large areas to accommodate a wide range of interface geometries.[15] The next section of this paper introduces a comprehensive review of past work on CNT thermal properties.

The thermomechanical strain in thermoelectric conversion systems can be significantly larger than in microprocessors. This calls for greater TIM thickness and increases the potential benefits of a nanostructured interface solution. In a typical thermoelectric module, solder is used to make electrical contact to the pellets and thermal grease is used to improve thermal contact between the module and surrounding surfaces. We attempt here to illustrate the different property requirements of interface materials in thermoelectric systems relative to the more mature microprocessor applications. The maximum shear stress σ experienced by an interface material can be estimated using[16]

$$\sigma = \Delta T(\alpha_1 - \alpha_2)\left(\frac{GL}{2d}\right). \quad (1)$$

ΔT is the temperature excursion from the zero-stress condition, α_1 and α_2 are the thermal expansion coefficients of the substrates, G is the shear modulus, L is the joint length, and d is the bond line thickness (BLT). This equation assumes that the TIM is relatively thick and flexible and that the substrates are unyielding. This equation gives an upper bound for the stress, since it does not account for the strain capabilities of the materials, but represents a reasonable approximation for comparison. Table I lists representative system parameters associated with TEGs and microprocessors. ΔT reflects the difference between off and on states. The TEG values are adapted from studies of waste heat recovery modules described in Vasquez et al.[17] The values for the BLT and microprocessor geometry are well documented in the literature.[11] Figure 1 shows the stresses resulting from using the values in Table I in Eq. 1 as well as the relation between thermal resistivity (R) and G for each TIM. For fixed values of ΔT, α_1, α_2, L, and d, stress increases with G of the TIM. The solid lines in Fig. 1 show that TEGs experience much higher stresses than microprocessors. The TEG pellet–metal interface has relatively low stress due to the small contact area but is still susceptible to fracture, as many thermoelectric materials are brittle. The boxed areas in Fig. 1 illustrate the tradeoff between mechanical and

Table I. Comparison of interfaces in representative microprocessor and thermoelectric material sets

Interface	ΔT (K)	CTE Mismatch (10^{-6}/K)	Common Joint Length (cm)	BLT (μm)
Microprocessor chip (Si) and heat spreader (Cu)	100	14	2	30
TEG module (Al_2O_3) and heat source (Cu)	600	8.5	7.5	100
TEG pellet (PbTe) and metal (Cu)	600	3.9	0.5	60

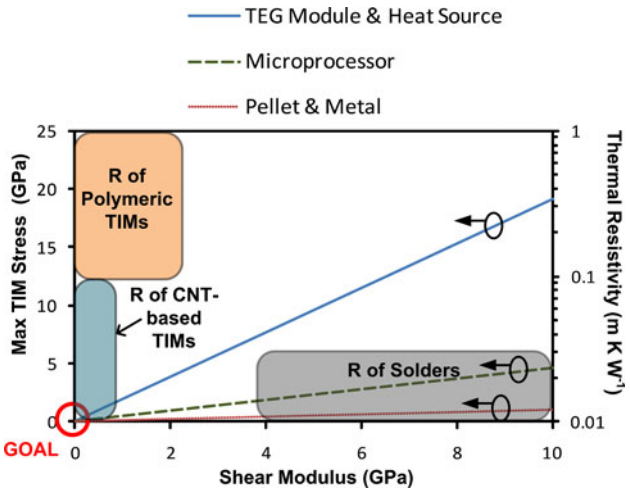

Fig. 1. *Lines*: maximum TIM stresses (σ) in TEG and microprocessor applications based on values from Table I. Polymeric TIMs range from particle-filled oils to epoxies, with shear modulus in the 0 GPa to 2 GPa range. The modulus of solders range from roughly 4 GPa (e.g., pure In) to 10 GPa (e.g., hard solders). *Boxes*: thermal resistivity (R) values (*right axis*, log scale) for CNT-based TIMs, polymeric TIMs, and solders.

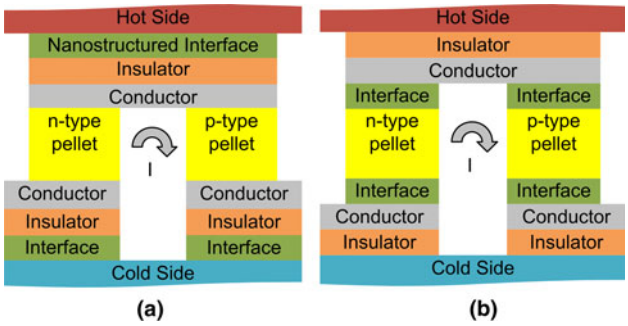

Fig. 2. (a) A nanostructured interface material ("Interface") is used around the module; (b) a nanostructured interface material ("Interface") is used between the thermoelectric material and metal leads. Figures are based on typical TEG construction.

thermal properties in polymeric TIMs and solders. High G corresponds to solders, while low G is characteristic of polymeric TIMs such as greases and gels. Comparison of σ and R shows that, although polymers may experience low stress, they typically have high R, while solders have very low R but high modulus and high stress. CNT-based TIMs approach the ideal TIM that minimizes σ, G, and R.

The solution to the thermal interface problem in thermoelectrics may be to apply CNT-based TIMs around the entire module (Fig. 2a) or between the pellet and electrical leads (Fig. 2b). The present work studies the unique implementation of CNT array interface materials grown directly on a thermoelectric material, as in Fig. 2b. In this work we characterize thermal properties of metal-coated aligned multiwalled carbon nanotube (MWCNT) films on SiGe, a standard high-temperature thermoelectric material,[18] using a nanosecond thermoreflectance technique.

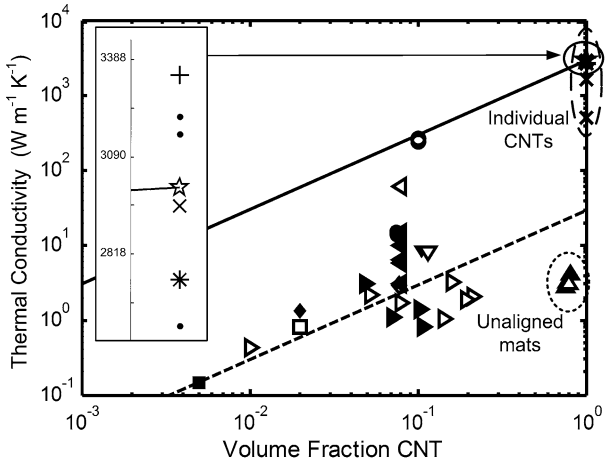

Vertically Aligned CNT Arrays:	Compressed Vertically Aligned CNT Arrays:	Individual CNTs:
● Yang et al.[29, 30]	▶ Marconnet – 1D Compressed.[39]	• Wang et al.[20]
○ Tong et al.[13, 36]	▷ Marconnet – 2D Compressed.[39]	x Fujii et al.[21]
■ Wang et al.[31]		☆ Kim et al.[22]
□ Pal et al.[32]	**Unaligned CNT Mats:**	+ Yu et al.[23]
◆ Son et al.[37]	▲ Zhang et al.[40]	✳ Pop et al.[24]
◇ Xu et al.[38]	△ Zhang et al.[41]	
▼ Borca-Tasciuc et al.[33]		
▽ Panzer et al.[12]		
◀ Ivanov et al.[34]		
◁ Xie et al.[35]		

Fig. 3. Thermal conductivity versus volume fraction of CNTs. The *solid line* is the predicted film thermal conductivity based on individual nanotubes with 3000 W m^{-1} K^{-1}. The *dashed line* is the predicted film thermal conductivity based on individual nanotubes with 30 W m^{-1} K^{-1}.

THERMAL CONDUCTION BY ALIGNED CNT FILMS

The excellent in-plane thermal conductivity of graphene sheets[19] suggests that CNTs should also possess high thermal conductivity, k. Recent experimental measurements of individual CNT k have shown values ranging from 500 W m^{-1} K^{-1} to 3200 W m^{-1} K^{-1}.[20–24] Arrays of vertically aligned CNTs can potentially take advantage of the high axial k of individual tubes but are limited in part by the low packing fraction of CNTs in the array and the interface resistance at the CNT–substrate contacts.[12,25] Several research groups are working to investigate and improve the thermal properties of vertically aligned CNT arrays.[12,13,26–38] Effective k values of vertically aligned CNT arrays reported in the literature range from 0.145 W m^{-1} K^{-1} to 267 W m^{-1} K^{-1}.[13,31]

A simple model of the aligned CNT arrays as conductors in parallel suggests that k should scale with the packing fraction. Figure 3 shows k of CNT samples from the literature as a function of the volume fraction of CNTs. Sample sets "Marconnet—1D Compressed" and "Marconnet—2D Compressed" are vertically aligned CNT arrays which were mechanically compressed to increase the packing fraction.[39] Although there is no clear trend

with increasing density from these samples, the effective k is lower than predicted by the volume fraction. Sample sets "Zhang et al." of unaligned CNT mats densified to a volume fraction near 0.80 had relatively low k despite the densification.[40,41] The thermal diffusivity in CNT arrays is highly anisotropic,[32–34] suggesting that tangled mats have lower thermal performance than aligned arrays.

Data from experimental measurements of individual nanotubes are located on the right axis corresponding to a volume fraction of 1, with average k around 3000 W m^{-1} K^{-1}. The majority of the vertically aligned CNT arrays discussed in the literature fall well below the predicted array k based on volume fraction with an individual nanotube k of 3000 W m^{-1} K^{-1} (solid line). In fact, many of the samples suggest an individual CNT k on the order of 30 W m^{-1} K^{-1} (dashed line), indicating that factors beyond the low density of vertically aligned CNT arrays, such as interface resistances between the CNT array and surrounding materials, degrade thermal performance. However, the high k values exceeding 250 W m^{-1} K^{-1} at ~10% volume fraction reported by Tong et al.[13,36] show promise for vertically aligned CNT arrays which take full advantage of high k values reported for individual CNTs.

EXPERIMENTAL PROCEDURES

Sample Preparation

Among the wide variety of thermoelectric materials available, this study aimed to work with one that has both technical promise and compatibility with the CNT growth process. SiGe substrates were chosen for their ability to withstand CNT growth temperatures of over 800°C. The SiGe samples were fabricated using molecular beam epitaxy on Si substrates and consist of a 2 μm buffer layer, a 1.3 μm superlattice of alternating Si and Ge, and a 0.3 μm highly doped cap layer.[42] The samples were then prepared for the CNT growth process, which was refined for high growth yield on SiGe substrates. Sample sets were prepared both with and without an initial 100-nm-thick plasma-enhanced chemical vapor deposition (PECVD) SiO_2 layer deposited on the SiGe substrate. Successful growth on both sample sets indicates that this SiO_2 layer is not necessary for MWCNT growth on SiGe. Next a 20 nm Al_2O_3 layer followed by a 10-Å-thick Fe film is deposited on all samples. Annealing in oxygen produces a monolayer of Fe clusters to act as catalysts for the CNT growth. A CVD system (Lindberg/Blue M Mini-Mite) was used for MWCNT synthesis. The furnace temperature was maintained at 825°C while a mixture of C_2H_4 and Ar gases flowed through the chamber for 30 min to produce an array of aligned nanotubes of ~1.5 μm height.

Figure 4a shows a schematic of the samples used in our measurements, including the locations of the measured boundary resistances. A 50-nm-thick platinum film is deposited on the CNT array for thermoreflectance measurements. The scanning electron microscopy (SEM) profile of the sample in Fig. 4b shows that the platinum layer uniformly coats the tops of the CNTs, with negligible voids. Figure 4c shows that the height of the CNT film is roughly 1.5 μm. Figure 4d shows that the rough surface of the CNT film can make thermoreflectance measurements difficult, as discussed below.

Measurement Techniques

Previous work has extensively described and applied the nanosecond thermoreflectance technique to measure the thermal properties of thin-film materials and their interfaces.[12] Figure 5 shows a schematic of the thermoreflectance system used in this work. In brief, 6 ns pulses at 532 nm wavelength from a Nd:YAG laser operating at 10 Hz heat the top metal film with a spot diameter of ~3 mm, creating a transient temperature field in the multilayer stack. The reflected intensity of a continuous-wave probe laser (658 nm wavelength) is proportional to the surface temperature[43] and provides a dynamic measurement of the surface temperature of the metal film. The probe laser is focused on the sample with a Gaussian $1/e^2$ width of ~20 μm, and a 650-MHz-bandwidth photodiode measures the reflected probe beam intensity. Since the heating diameter is much larger than the maximum thermal diffusion depth during the experiments, analysis reduces to a solution of the one-dimensional heat diffusion equation for a multilayer stack with surface heating that explicitly incorporates interface resistances.[12,44] A multiparameter least-squares fit of the transient thermal response data to the solution of the thermal model extracts the effective thermal properties of the CNT film.[12,44]

The surface topography and porous structure of the metal-coated MWCNT film as shown in Fig. 4 can potentially pose challenges for thermoreflectance techniques. Due to porosity, optical radiation may be absorbed on both the surface of the metal film and within the pores. However, since the thermal diffusion time scales in the metal film are much less than the temporal resolution capabilities of the measurement, it is inconsequential whether the heat is absorbed strictly on the surface of the metal or within its pores. Since voids in the metal coating are negligible and the metal is optically thick, the transmission of the pump and probe beams is insignificant.

The short timescales and unique time-dependent sensitivity of the thermal response to the thermal properties of the CNT film enable depth profiling of thermal resistances within the film and at its interfaces.[12] A comprehensive study of the impact of the variations in the thermal and physical properties (thickness) of each layer in the sample indicates that it is possible to extract the volumetric heat capacity of the CNT film $C_{v,\mathrm{eff}}$ and the boundary resistances $R''_{\mathrm{CNT-Pt}}$ and $R''_{\mathrm{CNT-Sub}}$. These values

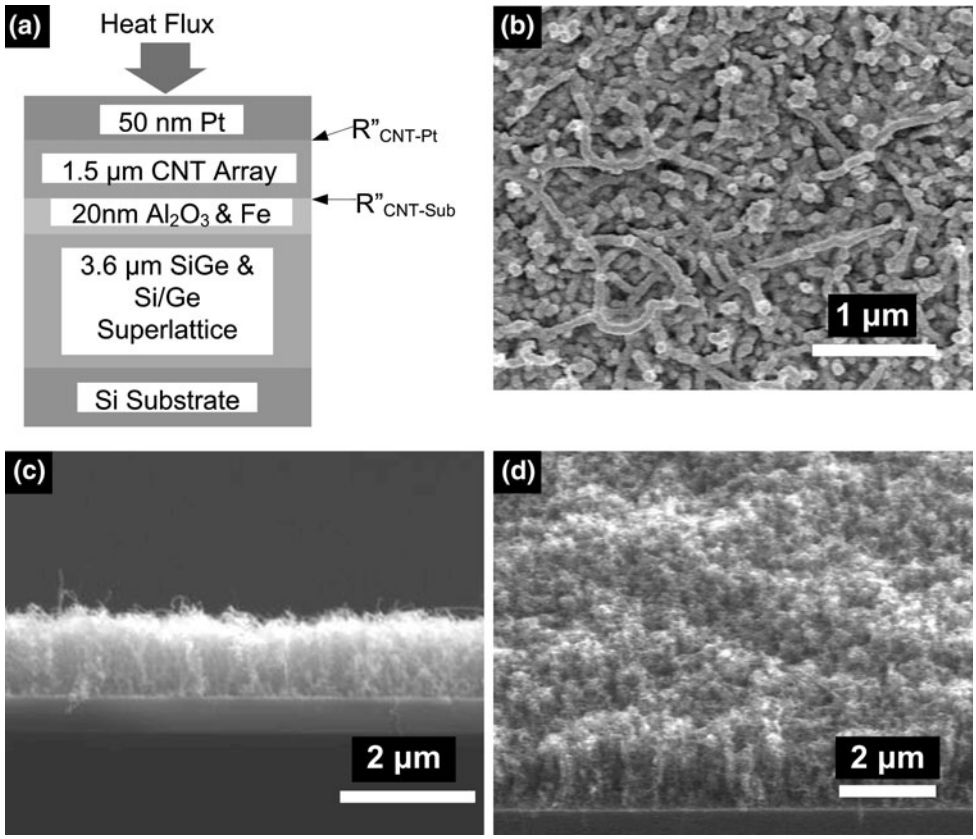

Fig. 4. (a) Schematic of sample geometry. A metal layer is deposited on the CNT array for thermoreflectance thermometry; (b) 50 nm Pt deposited on top of CNTs, showing minimal voids; (c) and (d) cross-sectional view and 45° view SEM images of CNT grown on SiGe/Si substrates before metallization.

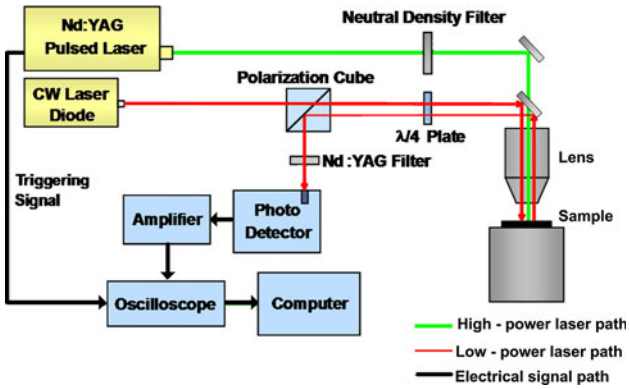

Fig. 5. Schematic of the laser setup, including the pump beam and probe beam paths.

can be individually resolved because each value uniquely affects the shape of the thermal response and appears separately in the analytic solution. The experimental error and uncertainty are due to a variety of factors including signal noise and uncertainty in the material parameters that affect the extracted values. These material parameters include the local variations in the metal thickness, CNT thickness, and interface microstructure. The analytic solution is not sensitive to the thermal conductivity of the metal layer and CNT layer or any properties of the SiGe layer and Si substrate. The insensitivity to the CNT conductivity and SiGe properties is advantageous due to the uncertainty associated with these values. The insensitivity to CNT conductivity is due to the large boundary resistances which dominate total resistance.[12,13,25,26] By assuming an approximate lower bound of $\sim$1 W m^{-1} K^{-1} for the effective thermal conductivity of the CNT array and an upper bound CNT thickness of 3 μm for the films used in this work, we can estimate an approximate upper bound of $\sim$3 m^2 K MW^{-1} for the CNT volumetric resistance, which is much lower than the measured values of boundary resistance in this work.

We measured the evolution of the thermal properties due to thermal cycling by mounting the sample on a programmable INSTEC® temperature-controlled stage. After applying 100 thermal cycles between 30°C to 200°C, the sample was measured using the same methods described above. The length of each cycle was roughly 6 min.

RESULTS AND DISCUSSION

Figure 6 shows a representative thermal response trace for the 1.5-μm-thick CNT film grown on SiGe along with the best-fit analytical solution (dashed line). Table II shows the fitted parameters before

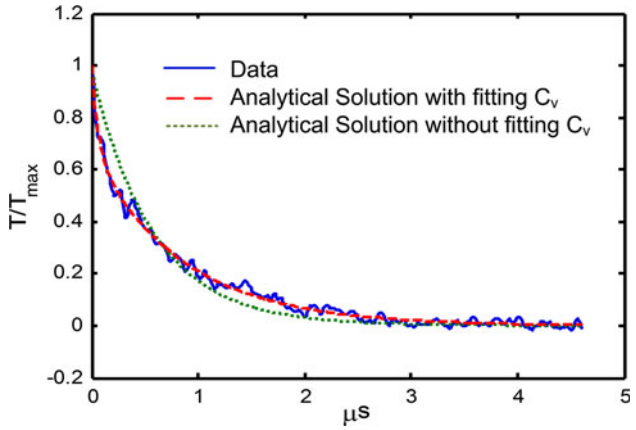

Fig. 6. Thermal response trace data (*solid*) and best-fit analytical solution (*dashed*) for CNTs grown on SiGe film measured with the nanosecond thermoreflectance system. T/T_{max} is normalized surface temperature. The *dotted line* shows a poor fit when the CNT layer is fitted as a lumped total resistance.

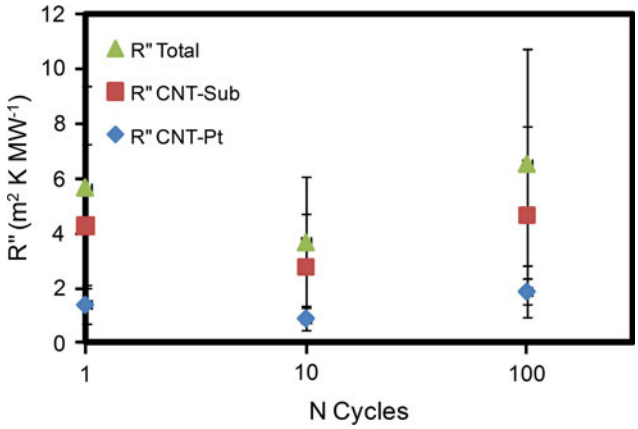

Fig. 7. Effect of thermal cycling from 30°C to 200°C on CNT film boundary resistances. *N* is the number of cycles.

Table II. Averaged best-fit values for the extracted properties of the CNT film grown on SiGe/Si substrate

Parameter	Average Result	Uncertainty (%)
R''_{CNT-Pt}	1.4 m^2 K MW^{-1}	50
$R''_{CNT-Sub}$	4.3 m^2 K MW^{-1}	70
$C_{v,eff}$	87 kJ m^{-3} K^{-1}	30

thermal cycling averaged over multiple measurements at three locations on the sample, as well as the uncertainty associated with each value. The dotted line in Fig. 6 shows that the analytical solution gives a poor fit when fitting the CNT layer only as a single resistance, without also fitting the volumetric heat capacity of the layer, $C_{v,eff}$. The need to simultaneously fit $C_{v,eff}$, R''_{CNT-Pt}, and $R''_{CNT-Sub}$ proves that the measurement is sensitive to the individual boundary resistances rather than a lumped total resistance of the array. We can estimate the effective fill fraction f_{eff} of the CNT film by comparing $C_{v,eff}$ to the volumetric heat capacity of an individual MWCNT $C_{v,ind}$.[12] The heat capacity c_p of MWCNTs is taken to be that of graphite, 710 J kg^{-1} K^{-1},[35] and the density ρ is 1.34×10^3 kg m^{-3},[30] giving $C_{v,ind}$ of roughly 1 MJ m^{-3} K^{-1}. Then f_{eff} is given by

$$f_{eff} = \frac{C_{v,eff}}{C_{v,ind}}. \quad (2)$$

The measured value of $C_{v,eff}$ gives an f_{eff} of 9%. MWCNT arrays typically have 0.5% to 10% volume fraction.[13,31] The values of k and ρ used in the data fitting are adjusted by multiplying single CNT properties by f_{eff}. The uncertainty in R''_{CNT-Pt} and $R''_{CNT-Sub}$ are due mainly to variations across the sample and uncertainty in the Pt thickness. The uncertainty in $C_{v,eff}$ is due largely to the uncertainty in CNT height, which is estimated to be between 1 μm and 3 μm based on SEM images.

The best-fit values for R''_{CNT-Pt} and $R''_{CNT-Sub}$ give a total boundary resistance R''_{tot} of 5.7 m^2 K MW^{-1}. This matches with previously reported boundary resistance values, which are typically between 1 m^2 K MW^{-1} and 100 m^2 K MW^{-1} for MWCNT arrays.[13,37] The relatively high boundary resistances may be due to poor adhesion of the Pt to the CNTs or delamination of some CNTs from the substrate, which can cause some tubes to make incomplete thermal contact. In practical applications of the CNT film, the boundary resistances may be reduced with the use of a eutectic-based binder material that maintains good thermal contact with more tubes.[13] The current value of R''_{tot} is analogous to a 17 μm layer of thermal grease at k = 3 W m^{-1} K^{-1}. It is often not possible to achieve such thin interfaces in thermoelectric systems. CNT-based TIMS are particularly competitive against traditional TIMs when thicker bond lines are necessary; the boundary resistances are less dominant, and mechanical compliance increases.

Results of thermal cycling of the same sample are shown in Fig. 7. There seems to be little effect on thermal resistance after ten cycles. There is roughly a 15% increase in $R''_{CNT-Sub}$ after 100 cycles, but this difference is still within the error range and not necessarily an indication of sample damage. Further study is needed to confirm the effects of thermal cycling.

CONCLUSIONS

This paper addresses the different interface requirements between thermoelectric and microprocessor applications and studies the relevance of using CNT thermal interface materials for thermoelectric systems. We explain the benefits of using a nanostructured TIM, demonstrate CNT growth on thermoelectric material, and measure the thermal boundary resistances and heat capacity associated

with the CNT film. The results show that the interfaces resistances around the CNT film are dominant, with R''_{CNT-Pt} of 1.4 m^2 K MW^{-1}, $R''_{CNT-Sub}$ of 4.3 m^2 K MW^{-1}, and $C_{v,eff}$ of 87 kJ m^{-3} K^{-1}. The boundary resistances can be reduced in future studies by the application of adhesion layers around the CNT film and by improving the CNT growth. It was found that thermal cycling does not have a significantly detrimental effect on the CNT array, though further studies are necessary as well as comprehensive imaging of the sample before and after cycling. Future work will also include a study of nanostructured interfaces in actual thermoelectric devices.

ACKNOWLEDGEMENTS

This research was funded in part by Bosch LLC, the Precourt Energy Efficiency Center, and the National Science Foundation. Special thanks go to Ali Shakouri's group at UC Santa Cruz for the SiGe substrates and Molecular Nanosystems Inc. for their CNT fabrication support.

REFERENCES

1. V. Ravi, S. Firdosy, T. Caillat, E. Brandon, K. Van Der Walde, L. Maricic, and A. Sayir, *J. Electron. Mater.* 38, 1433 (2009).
2. M. Srinivasan and S.M. Praslad, *Proceedings of the International Conference on Power Electronics and Drive Systems* (Kualu Lumpur, Malaysia), vol. 2, pp. 977–982, Institute of Electrical and Electronics Engineers Inc., Piscataway, NJ (2005).
3. X.C. Xuan, K.C. Ng, C. Yap, and H.T. Chua, *Int. J. Heat Mass Tran.* 45, 5159 (2002).
4. G. Min and D.M. Rowe, *Solid State Electron.* 43, 923 (1999).
5. T.J. Hendricks and J.A. Lustbader, *Proceedings of the 21st International Conference on Thermoelect.* (2002).
6. I. Chowdhury, R. Prasher, K. Lofgreen, G. Chrysler, S. Narasimhan, R. Mahajan, D. Koester, R. Alley, and R. Venkatasubramanian, *Nat. Nano* 4, 235 (2009).
7. A. Pettes, M. Hodes, and K. Goodson, *Proc. IPACK2007* 2, 221 (2007).
8. S. LeBlanc, Y. Gao, and K. Goodson, *Proceedings of IMECE 2008*, October 31–November 6, Boston, Massachusetts (2008).
9. T. Clin, S. Turenne, D. Vasilevskiy, and R. Masut, *J. Electron. Mater.* 38, 994 (2009).
10. Y. Hori, D. Kusano, T. Ito, and K. Izumi, *Proceedings of the 18th International Conference on Thermoelect*., p. 328 (1999).
11. R. Prasher, *Proc. IEEE* 94, 1571 (2006).
12. M.A. Panzer, G. Zhang, D. Mann, X. Hu, E. Pop, H. Dai, and K.E. Goodson, *J. Heat Transf.* 130, 052401 (2008).
13. T. Tong, Z. Yang, L. Delzeit, A. Kashani, M. Meyyappan, and A. Majumdar, *IEEE Trans. Compon. Pack. Technol.* 30, 92 (2007).
14. O. Yaglioglu, R. Martens, A. Hart, and A. Slocum, *Adv. Mater.* 20, 357 (2008).
15. G. Zhang, D. Mann, L. Zhang, A. Javey, Y. Li, E. Yenilmez, Q. Wang, J.P. McVittie, Y. Nishi, J. Gibbons, and H. Dai, *Proc. Natl Acad. Sci. USA* 102, 16141 (2005).
16. E.M. Petrie, *Handbook of Adhesives and Sealants* (New York: McGraw-Hill, 2000).
17. J. Vázquez, M.A. Sanz-Bobi, R. Palacios, and A. Arenas, *Proceedings of the 7th European Workshop Thermoelect.* (2002).
18. C.M. Bhandari and D.M. Rowe, *Contemp. Phys.* 21, 219 (1980).
19. R.S. Ruoff and D.C. Lorents, *Carbon* 33, 925 (1995).
20. Z.L. Wang, D.W. Tang, X.B. Li, X.H. Zheng, W.G. Zhang, L.X. Zheng, Y.T. Zhu, A.Z. Jin, H.F. Yang, and C.Z. Gu, *Appl. Phys. Lett.* 91, 123119 (2007).
21. M. Fujii, X. Zhang, H. Xie, H. Ago, K. Takahashi, T. Ikuta, H. Abe, and T. Shimizu, *Phys. Rev. Lett.* 95, 065502 (2005).
22. P. Kim, L. Shi, A. Majumdar, and P.L. McEuen, *Phys. Rev. Lett.* 87, 215502 (2001).
23. C. Yu, L. Shi, Z. Yao, D. Li, and A. Majumdar, *Nano Lett.* 5, 1842 (2005).
24. E. Pop, D. Mann, Q. Wang, K.E. Goodson, and H. Dai, *Nano Lett.* 6, 96 (2006).
25. B.A. Cola, J. Xu, C. Cheng, X. Xu, T.S. Fisher, and H. Hu, *J. Appl. Phys.* 101, 054313 (2007).
26. X.J. Hu, A.A. Padilla, J. Xu, T.S. Fisher, and K.E. Goodson, *J. Heat Transf.* 128, 1109 (2006).
27. S. Shaikh, K. Lafdi, and E. Silverman, *Carbon* 45, 695 (2007).
28. Y.M. Choi, S. Lee, H.S. Yoon, M.S. Lee, H. Kim, I. Han, Y. Son, I.S. Yeo, U.I. Chung, and J.T. Moon, *6th IEEE Conference on Nanotechnology* (2006).
29. D.J. Yang, S.G. Wang, Q. Zhang, P.J. Sellin, and G. Chen, *Phys. Lett. A* 329, 207 (2004).
30. D.J. Yang, Q. Zhang, G. Chen, S.F. Yoon, J. Ahn, S.G. Wang, Q. Zhou, Q. Wang, and J.Q. Li, *Phys. Rev. B* 66, 165440 (2002).
31. X. Wang, Z. Zhong, and J. Xu, *J. Appl. Phys.* 97, 064302 (2005).
32. S.K. Pal, Y. Son, T. Borca-Tasciuc, D.A. Borca-Tasciuc, S. Kar, R. Vajtai, and P.M. Ajayan, *J. Mater. Res.* 23, 2099 (2008).
33. T. Borca-Tasciuc, S. Vafaei, D.A. Borca-Tasciuc, B.Q. Wei, R. Vajtai, and P.M. Ajayan, *J. Appl. Phys.* 98, 054309 (2005).
34. I. Ivanov, A. Puretzky, G. Eres, H. Wang, Z. Pan, H. Cui, R. Jin, J. Howe, and D.B. Geohegan, *Appl. Phys. Lett.* 89, 223110 (2006).
35. H. Xie, A. Cai, and X. Wang, *Phys. Lett. A* 369, 120 (2007).
36. T. Tong, A. Majumdar, Z. Yang, A. Kashani, L. Delzeit, and M. Meyyappan, *ITHERM '06* (2006).
37. Y. Son, S.K. Pal, T. Borca-Tasciuc, P.M. Ajayan, and R.W. Siegel, *J. Appl. Phys.* 103, 024911 (2008).
38. J. Xu and T.S. Fisher, *Int. J. Heat Mass Trans.* 49, 1658 (2006).
39. A.M. Marconnet, personal communication, Dept. of Mechanical Engineering, Stanford University (2009).
40. H.L. Zhang, J.F. Li, K.F. Yao, and L.D. Chen, *J. Appl. Phys.* 97, 114310 (2005).
41. H.L. Zhang, J.F. Li, B.P. Zhang, K.F. Yao, W.S. Liu, and H. Wang, *Phys. Rev. B* 75, 205407 (2007).
42. A. Shakouri, *Proc. IEEE* 94, 1613 (2006).
43. B.M. Clemens, G.L. Eesley, and C.A. Paddock, *Phys. Rev. B* 37, 1085 (1988).
44. D.G. Cahill, *Rev. Sci. Instrum.* 75, 5119 (2004).